Supporting Information: Observation of graphene bubbles and effective mass transport under graphene films

E. Stolyarova[1†], D. Stolyarov[2†], K. Bolotin[3], S. Ryu[1], L. Liu[1], K. T. Rim, D. Eom, M. Klima[4], M. Hybertsen[5], I. Pogorelsky[2], I. Pavlishin[2], K. Kusche[2], J. Hone[4], P. Kim[3], H. L. Stormer[6], V. Yakimenko[2], G. Flynn[1*]

Generation of High Energy Protons by the Laser Driven Source

Laser driven sources of collimated high-energy ion beams constitute low-cost, compact devices in comparison to conventional particle accelerators.[1] To date these ion sources have been proposed for possible use in proton cancer therapy,[2] fusion energy research[3] and laboratory investigations of extreme states of matter.[4] Compared to conventional ion accelerators, laser driven high energy ion sources are especially well suited for materials science research since tailoring the foil target material allows a broad variety of ions to be controllably produced.[1, 5]

High energy ion beams are a powerful nanoscience tool that has already been successfully exploited to achieve controlled modification of carbon-based materials[6]. In particular, irradiation of graphite with a proton beam is of great interest due to the recent discovery of radiation induced magnetism.[7] In the present experiments a proton beam, derived from laser-driven ion acceleration generated by irradiation of a thin metal foil with an intense laser source, has been employed.[8] The principle of this process is illustrated in Figure 1 SUB. The ion acceleration is possible only for ultra-high intensity laser fields with the normalized vector potential $a_0>1$ indicating that laser-matter interaction proceeds in the relativistic regime.

Electrons, pushed through the foil by the laser field ponderomotive potential, form a negatively charged cloud at the backside of the foil. If the laser intensity is high enough, the static electric field created between the electron cloud and the foil ionizes impurities (mostly water and hydrocarbons) on the surface of the foil and accelerates these resulting ions.[8] The ions can also be accelerated directly by the laser field ponderomotive potential. (The latter is the dominant acceleration mechanism in the case of a circularly polarized laser beam[9].) The method of forming high energy charged beams used here combines direct ponderomotive acceleration by the laser field with acceleration due to the Coulomb potential arising from the electron cloud at the backside of the foil.

The laser-driven ion source used in the present experiments is based on the picosecond CO_2 laser system operated at the Accelerator Test Facility, Brookhaven National Laboratory[10]. Circularly polarized, 6 ps long laser pulses with an energy of about 5J are focused to a ~100 μm diameter spot at the surface of a 12 μm thick aluminum foil. The experimental setup is shown schematically in Figure 2 SUB. The accelerated ion beam passes through a 2-mm slit and 0.36 T permanent magnet thereby dispersing ions with different masses and energy. Modeling of ion motion shows that protons are well separated spatially from heavier ions. Protons enter the target at an incident angle of ~20°. All graphene samples were irradiated by protons generated from a single laser shot.

The silicon wafers with deposited graphene flakes were glued to the surface of CR-39 detectors (plastic plates sensitive to energetic ions) that were placed behind the magnet. Analysis of CR-39 plates allows exact assignment of the ion distribution and density on the carbon samples. Collisions of accelerated ions with a CR39 detector cause

localized radiation damage; etching of the material in the CR39 plate detector along the ion path is faster than etching in the other directions.[11] After irradiation, the samples were removed from the CR-39 plate, which was then etched in 6.5M KOH solution for 15 minutes. As a result of etching, pits, which are visible under an optical microscope, are formed in the detector plates.

A series of optical images was collected for different angles of deviation of the ions from a straight path (using a 250 μm step size), and individual pits were counted. This procedure allowed us to determine the composition, energy and flux of the ion beam. Protons with energy in the range 0.3-1MeV were found to be the major component of the accelerated ion beam; in addition Al^{n+}, C^{n+} (n=1...6) ions were observed. All graphene samples selected for this study were irradiated by a proton beam having energies in the 0.4-0.7 MeV range.

Calculations of pressure inside the bubble created by proton irradiation

The expression that relates deflection h of a round membrane with radius a to the gas pressure p under the membrane is given by the following equation: [12]

$$p = \left(1 - 0.24\nu\right)\frac{8}{3}\frac{Et}{\left(1-\nu\right)}\frac{h^3}{a^4} + 4\sigma_0 t\frac{h}{a^2} \quad (2)$$

where E=3 TPa is Young's modulus, ν= 0.4 is the Poisson ratio , σ_0 *is the* residual stress, and t =0.08 nm is the thickness of the graphene sheet [13]. The second term in this expression is proportional to the stress of the graphene sheet present in the film prior to bubble formation. [13] STM and AFM images collected under ambient conditions show no evidence of any considerable mechanical stress in the graphene films. Thus, we neglect this term in our pressure estimation. Using values of a=15 nm and h=0.7 nm as measured by AFM, the pressure in the bubble is found to be ~65 atm.

Expression (2) can only provide a rough estimate of the gas pressure. First of all, the calculated value of pressure depends strongly on both the height and radius of the bubble. Therefore, even small experimental errors in the measurement of these parameters lead to large uncertainty in the pressure value calculated using equation (2). In particular, the height of the bubbles is comparable with the substrate roughness, and the interaction of an AFM tip with the graphene film can distort the bubble causing an error in the measurement of the radius. In addition, Young modulus and the thickness of the membrane cannot be defined unambiguously for a graphene sheet. The values of these parameters have been shown to depend on the type of load imposed on the graphene sheet.[13] In the present experiments, the load varies from equibiaxial stretching on the top of the bubble to uniaxial stretching at the edges. In addition the behavior of the gas in such small cavities might significantly deviate form the ideal gas law.

Scanning probe studies and Raman Spectroscopy

AFM images were recorded in tapping mode (Veeco Multimode AFM) using Nanosensors™ AdvancedTEC™ NC AFM tips with a tip radius less than 10 nm. An optical microscope installed on top of the AFM setup allowed us to exactly position the AFM tip in the region that was being investigated by different techniques.

STM studies of the same flake were conducted under UHV and ambient conditions. The image shown in Fig. 1(c) was recorded in UHV at 77K with a base pressure of $2 \cdot 10^{-11}$ Torr. The scanning conditions are V_{bias}=-0.5 V and I_{set}=400 pA. Several hundred STM images were collected covering an approximately 3 μm^2 area. None of STM images revealed the $\sqrt{3} \times \sqrt{3}$ interference pattern expected when carbon atoms in the graphene network are displaced. [14] Such interference patterns are routinely

observed in STM images of bulk graphite bombarded by high energy heavy ions. [15-17] Therefore, the STM results are consistent with the view that the graphene lattice has not been altered by proton irradiation.

Raman measurements were performed in a backscattering geometry under ambient conditions. The output of an Ar ion laser (λ=514.5 nm) was focused to a ~1 μm^2 spot using a 40X objective. A detailed description of the Raman and STM apparatus has been given in previous publications.[18, 19]

HF/H_2O etching of SiO_2 under graphene

HF/H_2O etching is a standard technique used for removal of a SiO_2 layer from silicon wafers. [20] This method has been applied to the fabrication of suspended graphene devices with ultrahigh carrier mobility[21, 22] as the graphene film is not affected by the etching reagents while the silicon dioxide under the graphene is efficiently removed. This process can be used to remove completely or partially the 300 nm thick layer of silicon dioxide from the silicon dioxide/silicon wafer. In the experiments described here, the wafer was placed on top of a hot plate near a beaker filled with 40% HF solution. The temperature of the wafer was maintained at 50 °C. The etching rate of bare SiO_2 under these conditions was measured to be 20 nm/hour.

To ensure etching of SiO_2 under graphene, a constant supply of HF and water is required. The penetration of reactants into the SiO_2 regions covered by graphene can be explained either by passage of HF and H_2O molecules through the graphene or by their transport under the edge of the flake. The first scenario is not likely. The small openings in the graphene hexagonal lattice allow only penetration of atomic hydrogen and protons.[23] The penetration of all other species is possible only though diffusion. Even

through HF and water are among the smallest inorganic molecules, the molecular diameter of HF estimated from a hard sphere model is 2.12 Å, [24] and the molecular diameter of a water molecule is 2.75 Å. [25] On the other hand, the interatomic distance in a graphene lattice is only 1.42 Å [26], and , therefore, penetration of the reagents through the graphene film is unlikely.

In the second scenario, reactants efficiently move under the graphene sheet along the graphene-SiO_2 interface and initiate etching. Diffusion is well known to insure transport of molecules between graphene sheets in graphite crystals during the formation of intercalation compounds.[27] In the present experiments transport of reactants was confirmed by our observation that no etching was observed *under* the graphene sheet if the graphene edges are completely covered by a gold film and, therefore, protected from penetration by etching reagents through the sheet edges. [28]

Etching is described by the following reaction, if HF is supplied in gaseous form: [20, 29]

$$SiO_2 + 4HF \xrightarrow{water} SiF_4 + 2H_2O \quad (1)$$

Silicon tetrafluoride SiF_4 is a volatile gaseous compound at room temperature that easily escapes the surface. Water acts as a catalyst for this reaction and is required to form the transition state. [29] Habuka *et. al.* [30] have confirmed that reaction (1) is not observed in the absence of water vapor.

The efficiency of SiO_2 etching depends strongly on the experimental conditions, such as the partial pressures of HF and H_2O as well as the temperature of the SiO_2 substrate. If the partial pressures of HF and water vapor are high enough to form a multilayer aqueous film, the etching rate is similar to that observed in the liquid phase. If

the partial pressures of HF and H_2O are only sufficient for sub-monolayer coverage, the reaction proceeds in small liquid droplets formed on the SiO_2 surface. In this case, the etching is much less efficient and results in rough non-uniform surfaces.

Capture of water by the SiO_2 surface is the rate limiting step for reaction (1). The dependence of the etching rate on the concentration of water vapor can explain the higher reaction rate of SiO_2 covered by graphene compared to the rate for bare SiO_2. Under our experimental conditions high wafer temperatures cause fast water desorption from SiO_2 surfaces not covered by graphene, thereby preventing formation of a water film. Under these conditions the etching of bare SiO_2 is expected to proceed in small droplets on the surface.[20] On the other hand for SiO_2 covered with a graphene film, water formed by reaction (1) can remain trapped between the substrate and the graphene film and thereby accelerate etching.[20] This may explain the higher etching rate underneath the graphene film as observed in our experiments.

We found that incomplete removal of the thermally grown SiO_2 layer from a silicon wafer results in the formation of a porous, rough surface under the graphene film.[28] Effective sealing of gas at the SiO_2/graphene interface is unlikely for such a surface. This may account for the observation in the present experiments that bubble formation was observed only if the SiO_2 layer was completely removed from the silicon wafer.

Figure Captions for Support Materials:

Figure 1 sub. A schematic representation of the process describing the laser driven generation and acceleration of protons. An intense laser beam is directed at the surface of

the aluminum foil, and a plasma is formed as a result of interaction of the laser beam with the material of the foil.

Figure 2 sub. A schematic drawing of the experimental arrangement used for irradiation of graphene samples with the proton beam.

1. Hegelich, B. M.; Albright, B. J.; Cobble, J.; Flippo, K.; Letzring, S.; Paffett, M.; Ruhl, H.; Schreiber, J.; Schulze, R. K.; Fernundez, J. C. *Nature* **2006,** 439, (7075), 441-444.
2. Bulanov, S.; Khoroshkov, V. *Plasma Phys. Rep.* **2002,** 28, (5), 453-456.
3. Roth, M.; Cowan, T. E.; Key, M. H.; Hatchett, S. P.; Brown, C.; Fountain, W.; Johnson, J.; Pennington, D. M.; Snavely, R. A.; Wilks, S. C.; Yasuike, K.; Ruhl, H.; Pegoraro, F.; Bulanov, S. V.; Campbell, E. M.; Perry, M. D.; Powell, H. *Phys. Rev. Lett.* **2001,** 86, (3), 436.
4. Patel, P. K.; Mackinnon, A. J.; Key, M. H.; Cowan, T. E.; Foord, M. E.; Allen, M.; Price, D. F.; Ruhl, H.; Springer, P. T.; Stephens, R. *Phys. Rev. Lett.* **2003,** 91, (12), 125004.
5. Hegelich, M.; Karsch, S.; Pretzler, G.; Habs, D.; Witte, K.; Guenther, W.; Allen, M.; Blazevic, A.; Fuchs, J.; Gauthier, J. C.; Geissel, M.; Audebert, P.; Cowan, T.; Roth, M. *Phys. Rev. Lett.* **2002,** 89, (8), 085002.
6. Krasheninnikov, A. V.; Banhart, F. *Nat Mater* **2007,** 6, (10), 723-733.
7. Barzola-Quiquia, J.; Esquinazi, P.; Rothermel, M.; Spemann, D.; Butz, T.; Garcia, N. *Phys. Rev. B* **2007,** 76, (16), 161403-4.
8. Wilks, S. C.; Langdon, A. B.; Cowan, T. E.; Roth, M.; Singh, M.; Hatchett, S.; Key, M. H.; Pennington, D.; MacKinnon, A.; Snavely, R. A. *Phys. Plasm.* **2001,** 8, (2), 542-549.
9. Liseikina, T. V.; Macchi, A. *Appl. Phys. Lett.* **2007,** 91, (17), 171502.
10. Pogorelsky, I.; Pavlishin, I.; Yakimenko, V.; Shkolnikov, P.; Pukhov, A. *12 AAC Workshop. AIP Conf. Proc.* **2006,** 877, 409-15.
11. Dörschel, B.; Fülle, D.; Hartmann, H.; Hermsdorf, D.; Kadner, K.; Radlach, C. *Radiat Prot Dosimetry* **1997,** 69, (4), 267-274.
12. Alaca, B. E.; Selby, J. C.; Saif, M. T. A.; Sehitoglu, H. *Rev. Scie. Instr.* **2002,** 73, (8), 2963-2970.
13. Huang, Y.; Wu, J.; Hwang, K. C. *Phys. Rev. B* **2006,** 74, (24), 245413.
14. Mizes, H. A.; Foster, J. S. *Science* **1989,** 244, 559-562.
15. Liu, J.; Neumann, R.; Trautmann, C.; Müller, C. *Phys. Rev. B* **2001,** 64, (18), 184115.
16. Hahn, J. R.; Kang, H. *Phys. Rev. B* **1999,** 60, (8), 6007.
17. Yan, J.; Li, Z.; Bai, C.; Yang, W. S.; Wang, Y.; Zhao, W.; Kang, Y.; Yu, F. C.; Zhai, P.; Tang, X. *J. Appl. Phys.* **1994,** 75, (3), 1390.

18. Liu, L.; Ryu, S.; Tomasik, M. R.; Stolyarova, E.; Jung, N.; Hybertsen, M. S.; Steigerwald, M. L.; Brus, L. E.; Flynn, G. W. *Nano Lett.* **2008,** 8, (7), 1965.
19. Stolyarova, E.; Rim, K. T.; Ryu, S.; Maultzsch, J.; Kim, P.; Brus, L. E.; Heinz, T. F.; Hybertsen, M. S.; Flynn, G. W. *PNAS* **2007,** 104, (22), 9209-9212.
20. Hull, R., *Properties of Crystalline Silicon*. Forth ed.; IET: 1999.
21. Bolotin, K. I.; Sikes, K. J.; Jiang, Z.; Klima, M.; Fudenberg, G.; Hone, J.; Kim, P.; Stormer, H. L. *Solid State Comm.* **2008,** 146, (9-10), 351-355.
22. Du, X.; Skachko, I.; Barker, A.; Andrei, E. Y. *Nat Nano* **2008,** 3, (8), 491-495.
23. Waqar, Z. *J. Mat. Sci.* **2007,** 42, (4), 1169-1176.
24. Karger, N.; Ludemann, H. D. *J. Phys. Chem.* **1998,** 109, (9), 3301-3303.
25. Graziano, G. *Biophys. Chem.* **2003,** 104, (2), 393-405.
26. Sinitsyna, O. V.; Yaminsky, I. V. *Usp. Khim.* **2006,** 75, (1), 27-35.
27. Zabel, H.; Solin, S., *Graphite Intercalation Compounds I: Structure and Dynamics*. Springer-Verlag: 1990.
28. Bolotin, K. *in preparation* **2008**.
29. Kang, J. K.; Musgrave, C. B. *J. Chem. Phys.* **2002,** 116, (1), 275-280.
30. Habuka, H.; Otsuka, T. *Jpn. J. Appl. Phys.* **1998,** 118, 6123.

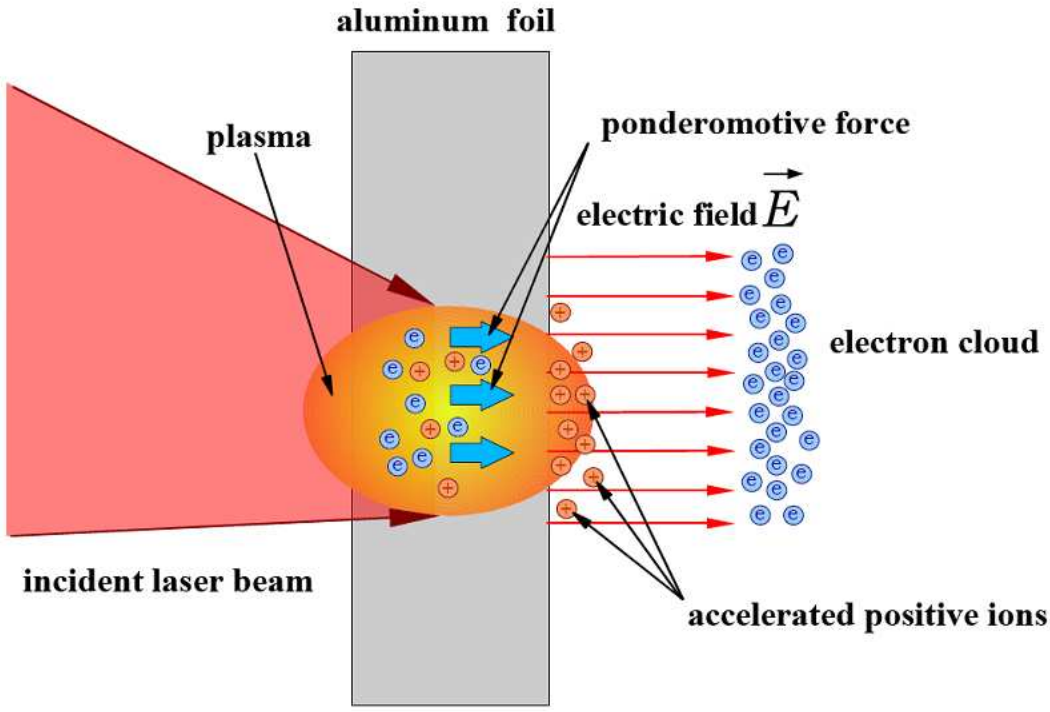

Figure 1SUP

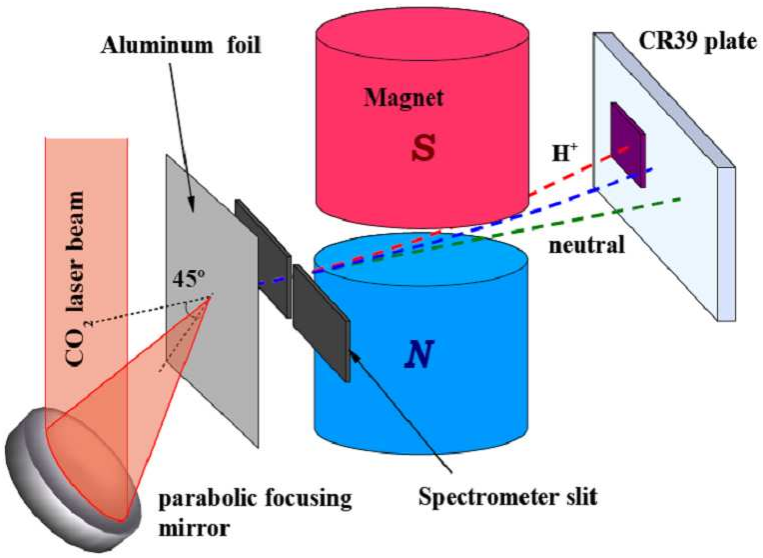
Aluminum foil
Magnet
S
CR39 plate
H+
neutral
CO2 laser beam
45°
N
parabolic focusing mirror
Spectrometer slit

Figure 2SUP